

Coherent states for graphene under the interaction of crossed electric and magnetic fields

M Castillo-Celeita^{*1}, E Díaz-Bautista^{†1,2}, and M Oliva-Leyva^{‡1}

¹Physics Department, Cinvestav, P.O. Box. 14-740, 07000 Mexico City, Mexico

²Departamento de Formación Básica Disciplinaria, Unidad Profesional Interdisciplinaria de Ingeniería Campus Hidalgo del Instituto Politécnico Nacional, Pachuca: Ciudad del Conocimiento y la Cultura, Carretera Pachuca-Actopan km 1+500, San Agustín Tlaxiaca, 42162 Hidalgo, Mexico

Abstract

We construct the coherent states for charge carriers in a graphene layer immersed in crossed external electric and magnetic fields. For that purpose, we solve the Dirac-Weyl equation in a Landau-like gauge avoiding applying techniques of special relativity, and thus we identify the appropriate rising and lowering operators associated to the system. We explicitly construct the coherent states as eigenstates of a matrix annihilation operator with complex eigenvalues. In order to describe the effects of both fields on these states, we obtain the probability and current densities, the Heisenberg uncertainty relation and the mean energy as functions of the parameter $\beta = c\mathcal{E}/(v_F B)$. In particular, these quantities are investigated for magnetic and electric fields near the condition of the Landau levels collapse ($\beta \rightarrow 1$).

1 Introduction

The allotropes of carbon, that present a variety of crystal structures from zero- to three-dimensional, have interesting and different properties. For instance, since the isolation of graphene, the main two-dimensional allotrope of carbon, by Novoselov and Geim [1, 2] there has been an avalanche of theoretical and experimental research about its physical properties and technological applications [3–7]. In a more general aspect, graphene has also attracted the attention to other two-dimensional Dirac materials (2D DMs) [8–13]. The graphene band structure is characterized by a linear behavior of the dispersion relation close to the so-called Dirac points, which are located at the Brillouin zone corners. As a consequence, its electrons are described by an effective massless Dirac equation with the Fermi velocity $v_F \sim c/300$ playing the role of the light speed c . In the case in which an external magnetic field is applied to a graphene sample on xy -plane, the system that arises is described by the Dirac-Weyl (DW) equation and has been employed not only in experimental researches but also in several theoretical works in which different magnetic field profiles are considered (for instance, see Refs. [14–19]). Nevertheless, when an electric field interacts with the above system the problem nature changes, so that it is necessary to implement either a numerical method or a process

*mfcastillo@fis.cinvestav.mx

†ediaz@fis.cinvestav.mx, ediazba@ipn.mx

‡mauriceoliva.cu@gmail.com

that involves rotations in order to solve the equations that appear [19–23]. For instance, for position-dependent electrostatic potentials $U(x)$, a relativistic approach is often used to become the problem into an analogous one of special relativity with a massless particle moving with an effective velocity v_F [24–26]. In general, the combined effect of magnetic and electric fields in graphene results an important research topic because it has given rise to new phenomena, such as the collapse of Landau levels [22, 24, 27, 28].

On the other hand, the physical system of a charged particle interacting with an electric and/or magnetic field is well-known in non-relativistic classical mechanics. For instance, when an electron stay in a plane and a magnetic field is applied, it describes a circular motion in the plane, while in the interaction with both magnetic and electric fields, it follows a spiral path on the plane. Thus, one would expect that it is possible to obtain a semi-classical description for the same field configuration in the graphene case by employing the so-called coherent states, which are states proposed by E. Schrödinger [29] as a kind of quantum states that described the motion of a particle in a quadratic potential and that minimize the Heisenberg uncertainty relation (HUR). Such states are considered as the most classical ones and have been employed and generalized to describe other physical systems, e.g., in quantum optics, atomic, nuclear, condensed matter and particle physics (see Refs. [30–33]). Inspired by this approach, part of this work consists of solving the problem of the interaction of a graphene sample with both magnetic and electric fields by performing a simple algebraic procedure, without the need to implement a Lorentz boost. Likewise, the coherent states construction for this case is motivated by the previous results of Refs. [34–36] and, ultimately, it seeks to expand the theoretical background for the description of a bit different system.

This work is presented as follows. In Sec. 2, we briefly discuss the classical motion equations of charged particles under the interaction of crossed electric and magnetic fields. In Sec. 3, the DW equation with a field configuration similar to that of the preceding section is solved. The energy spectrum and eigenvectors are found explicitly by implementing a non-relativistic approach, in contrast with previous works. In Sec. 4, a generalized annihilation operator is defined and the coherent states are constructed as its eigenstates with complex eigenvalues. In addition, the corresponding probability and current densities are described, and the effects of the electric field applied are analyzed through the Heisenberg uncertainty relation and mean energy. In Sec. 5 we present our final remarks and conclusions.

2 Charge carriers in classical fields

Let us suppose a particle of mass m and charge q moving on xy -plane interacting with crossed external electric and magnetic fields. The problem can be solved either by the Newtonian or Hamiltonian formalism in order to obtain the motion equations. By using the latter, the Hamiltonian H_{class} that describe this system is expressed as

$$H_{\text{class}} = \frac{1}{2m}(\mathbf{p} - \frac{q}{c}\mathbf{A})^2 + qU(x), \quad (1)$$

where the potentials are taking by $\mathbf{A} = Bx\hat{j}$ and $U(x) = -\mathcal{E}x$, such that $\mathbf{B} = \nabla \times \mathbf{A} = B\hat{k}$ and $\mathbf{E} = -\nabla U(x) = \mathcal{E}\hat{i}$, respectively. Considering an electron ($q = -e$), the solutions of the corresponding motion equations are given by

$$x(t) = x_0 + \frac{1}{\omega_B} [(v_{0y} + v_d) (\cos(\omega_B t) - 1) + v_{0x} \sin(\omega_B t)], \quad (2a)$$

$$y(t) = y_0 + \frac{1}{\omega_B} [(v_{0y} + v_d) \sin(\omega_B t) + v_{0x} (1 - \cos(\omega_B t))] - v_d t, \quad (2b)$$

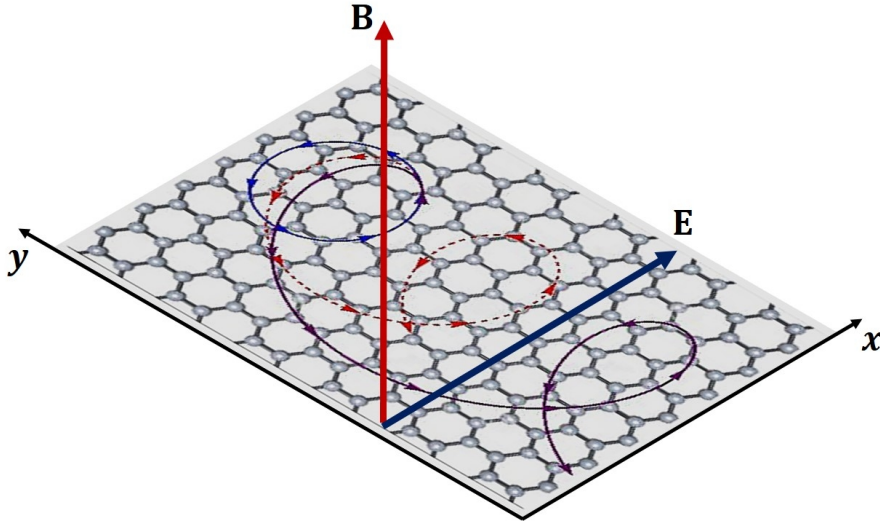


Figure 1: Graphene layer interacting with crossed electric and magnetic fields directed along the x - and z -directions, respectively. In absence of electric field \mathbf{E} , a classical charged particle performs a circular trajectory (blue curve), while if the strength \mathcal{E} increases, the trajectory becomes into a trochoid (red and purple curves).

where $\mathbf{r}_0 = (x_0, y_0)$ is the initial position of the particle, $\mathbf{v}_0 = (v_{0x}, v_{0y})$ denotes its initial velocity, $\omega_B = eB/mc$ is the cyclotron frequency and $v_d = c\mathcal{E}/B$ is the drift velocity.

From the above equations, we obtain the expression

$$\left(x(t) - x_0 + \frac{v_{0y} + v_d}{\omega_B}\right)^2 + \left(y(t) - y_0 + v_d t - \frac{v_{0x}}{\omega_B}\right)^2 = \frac{1}{\omega_B^2} [(v_{0y} + v_d)^2 + v_{0x}^2], \quad (3)$$

that corresponds to the equation of a circumference centered in the point

$$(h, k) = \left(x_0 - \frac{v_{0y} + v_d}{\omega_B}, y_0 - v_d t + \frac{v_{0x}}{\omega_B}\right), \quad (4)$$

and radius $R = \omega_B^{-1} \sqrt{(v_{0y} + v_d)^2 + v_{0x}^2}$. Here, the circle center moves along the y -axis with speed v_d . When the electric field \mathbf{E} is null, we have that $v_d = 0$ and Eq. (3) corresponds to circle equation with center in $(x_0 - v_{0y}/\omega_B, y_0 + v_{0x}/\omega_B)$ and radius $R = |\mathbf{v}_0|/\omega_B$. In presence of an electric field \mathbf{E} , instead of a circular motion, the trajectories describe a cycloidal motion along the y -axis. If the strength \mathcal{E} increases, the trajectories open further towards the negative x -axis (see Fig. 1).

On the other hand, the dynamics of relativistic particles is studied through appropriate Lorentz transformations that allow to find the motion equations in a coordinate frame S' moving with a velocity \mathbf{u} with respect to the original frame S . For the case with $\mathcal{E} < B$, the velocity \mathbf{u} is chosen perpendicular to the vectors \mathbf{E} and \mathbf{B} , so that the only field acting in the frame S' is \mathbf{B}' , and \mathbf{u} has a physical meaning as the drift velocity if $|\mathbf{u}|$ is less than c . For $\mathcal{E} > B$, it is necessary to perform a different Lorentz transformation from the frame S to a system S'' in which the only field acting is now \mathbf{E}' that causes a hyperbolic motion [37].

3 Dirac-Weyl equation with external fields

Now, let us consider a graphene layer laying on xy -plane interacting with external electric and magnetic fields, that are respectively parallel and orthogonal to the layer surface, as illustrated

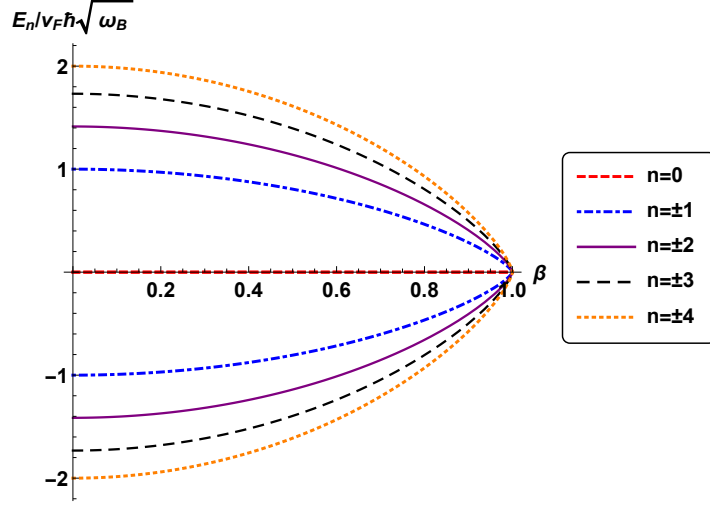


Figure 2: Plot of Landau levels (LLs) as a function of β and $k = 0$. For $\beta = 0$, the energy eigenstates lie on LLs, but as $\beta \rightarrow 1$, Landau level spectrum collapses.

in Fig. 1. The Hamiltonian that describes this problem is given by

$$H\bar{\Psi}(x,y) = \left[v_F \boldsymbol{\sigma} \cdot \left(\mathbf{p} + \frac{e}{c} \mathbf{A} \right) - eU(x) \right] \bar{\Psi}(x,y) = E\bar{\Psi}(x,y), \quad (5)$$

where $\bar{\Psi}(x,y) = \exp(iky) \Psi(x)$, the electrostatic and magnetic potentials are given again by $U(x) = -\mathcal{E}x$ and $\mathbf{A}(x) = Bx\hat{j}$, respectively, and $\boldsymbol{\sigma} = (\sigma_x, \sigma_y)$ are the Pauli matrices.

Thus, the above equation becomes:

$$\left[\left(\frac{E - e\mathcal{E}x}{\hbar v_F} \right) \mathbb{I}_2 + i\partial_x \sigma_x - \frac{1}{l_B^2} (x + l_B^2 k) \sigma_y \right] \Psi(x) = 0, \quad (6)$$

where \mathbb{I}_2 denotes the 2×2 unity matrix and the magnetic length l_B is given by $l_B^2 = 2/\omega_B = c\hbar/eB$. By introducing the parameter β and the dimensionless quantity ξ ,

$$\beta = \frac{e\mathcal{E}}{\hbar v_F} l_B^2 = \frac{c\mathcal{E}}{v_F B} = \frac{v_d}{v_F}, \quad \xi = \frac{1}{l_B} (x + l_B^2 k), \quad (7)$$

Eq. (6) can be rewritten as

$$\left[\left(\frac{E}{\hbar v_F} + k\beta - \frac{\beta\xi}{l_B} \right) \mathbb{I}_2 + \frac{i}{l_B} \frac{d}{d\xi} \sigma_x - \frac{\xi}{l_B} \sigma_y \right] \Psi(\xi) = 0, \quad (8)$$

which is solved in detail on Appendix A.

The energy spectrum E_n is given by [6, 22, 24, 26] (see Fig. 2):

$$E_{(1,n-1)} = E_{(2,n)} = \text{sgn}(n) \frac{\hbar v_F (1 - \beta^2)^{3/4}}{l_B} \sqrt{2n} - \hbar v_F k \beta, \quad (9)$$

where $\text{sgn}(0) = 1$, while the eigenspinors $\bar{\Psi}_n(x,y)$ can be expressed as:

$$\begin{aligned} \bar{\Psi}_n(x,y) &\equiv \bar{\Psi}_n(\zeta_n, y) = \frac{\exp(iky)}{\sqrt{2^{(1-\delta_{0n})}}} \left[(1 - \delta_{0n}) \psi_{n-1}(\zeta_n) \chi_{\lambda_1} + \eta \psi_n(\zeta_n) \chi_{\lambda_2} \right] \\ &= \frac{\exp(iky)}{\sqrt{2^{(1-\delta_{0n})}}} \sqrt{\frac{1}{2}} \begin{pmatrix} \sqrt{C_+} & i\sqrt{C_-} \\ -i\sqrt{C_-} & \sqrt{C_+} \end{pmatrix} \begin{pmatrix} (1 - \delta_{0n}) \psi_{n-1}(\zeta_n) \\ i\eta \psi_n(\zeta_n) \end{pmatrix} \\ &= \mathbb{M} \bar{\Phi}_n(x,y), \quad n = 0, 1, 2, \dots, \end{aligned} \quad (10)$$

Here, δ_{mn} denotes the Kronecker delta, $\eta = +$ for the K valley while $\eta = -$ for the K' valley,

$$\mathbb{M} = \sqrt{\frac{1}{2}} \begin{pmatrix} \sqrt{C_+} & i\sqrt{C_-} \\ -i\sqrt{C_-} & \sqrt{C_+} \end{pmatrix} = \sqrt{\frac{1}{2}} \left(\sqrt{C_+} \mathbb{I}_2 - \sqrt{C_-} \sigma_y \right), \quad (11a)$$

$$\bar{\Phi}_n(x, y) = \frac{\exp(iky)}{\sqrt{2(1-\delta_{0n})}} \begin{pmatrix} (1 - \delta_{0n})\psi_{n-1}(\zeta_n) \\ i\eta \psi_n(\zeta_n) \end{pmatrix}, \quad (11b)$$

with $C_{\pm} = 1 \pm (1 - \beta^2)^{1/2}$ and the wave functions are given by

$$\psi_n(x) \equiv \psi_n(\zeta_n) = \frac{(1 - \beta^2)^{1/8}}{\sqrt{n!}} \left(\frac{\omega_B}{2\pi} \right)^{1/4} D_n(\sqrt{2} \zeta_n), \quad (12)$$

where $D_n(z) = U(-n - \frac{1}{2}; z)$ designates the parabolic cylinder function and

$$\zeta_n = \xi(1 - \beta^2)^{1/4} - \frac{\beta \epsilon_0 l_B}{(1 - \beta^2)^{3/4}} = \frac{(1 - \beta^2)^{1/4}}{l_B} \left[x + l_B^2 k + \text{sgn}(n) \frac{\beta l_B \sqrt{2n}}{(1 - \beta^2)^{1/4}} \right]. \quad (13)$$

In Eq. (9), positive (negative) energies correspond to Dirac fermions in the conduction (valence) band. For $\beta = 0$ (*i.e.*, vanishing electric field), the spinors $\bar{\Phi}_n$ in (11) reduce to the solutions of standard Landau-like problem that was considered in Refs. [1, 2, 14, 15, 34], for instance. A brief comment about matrix \mathbb{M} can be found in Appendix B.

Figure 3 shows the behavior of the probability density $\rho_n(x)$ and y -current density $j_y(x)$ which were built with the eigenstates in (10) (see C). In particular, for $\beta = 0$, $\rho_n(x)$ is an even function while $j_y(x)$ is an odd function respect to reflection around a point x_0 such that $\xi|_{x=x_0} = 0$. However, as $\beta \rightarrow 1$ the parity breaks and the maximum values of both functions move in the negative x -direction. Furthermore, according to [14] the sign of $j_y(x)$ indicates the direction along the y -axis in which the electron motion takes place, so the current density behavior suggests there is a flux of probability in the negative y -direction when an electric field is applied to the sample. It is worth to mention that Figs. 3a and 3b are according with the results on [14].

Finally, according to [38, 39] the average velocity in the y -direction is given by

$$\langle v_y \rangle = \frac{1}{\hbar} \frac{\partial E_n}{\partial k} = -v_F \beta = -v_d = \left[\frac{\mathbf{E} \times \mathbf{B}}{B^2} \right]_y, \quad (14)$$

that means the Dirac fermions move with an average velocity v_d in the negative y -direction.

4 Annihilation operator

In order to build the coherent states associated with the problem, it is necessary to perform a transformation that allows us to work with an adequate set of eigenstates for which can be defined an annihilation operator, namely Θ^- . Thus, considering the inverse matrix \mathbb{M}^{-1} , we obtain:

$$\bar{\Phi}_n(x, y) = \mathbb{M}^{-1} \bar{\Psi}_n(x, y) = \frac{\exp(iky)}{\sqrt{2(1-\delta_{0n})}} \begin{pmatrix} (1 - \delta_{0n})\psi_{n-1}(\zeta_n) \\ i\eta \psi_n(\zeta_n) \end{pmatrix}. \quad (15)$$

In this representation, we can define the following differential operators

$$\theta_n^{\pm} = \frac{1}{\sqrt{2}} \left(\mp \frac{d}{d\zeta_n} + \zeta_n \right), \quad \theta_n^+ = (\theta_n^-)^{\dagger}, \quad (16)$$

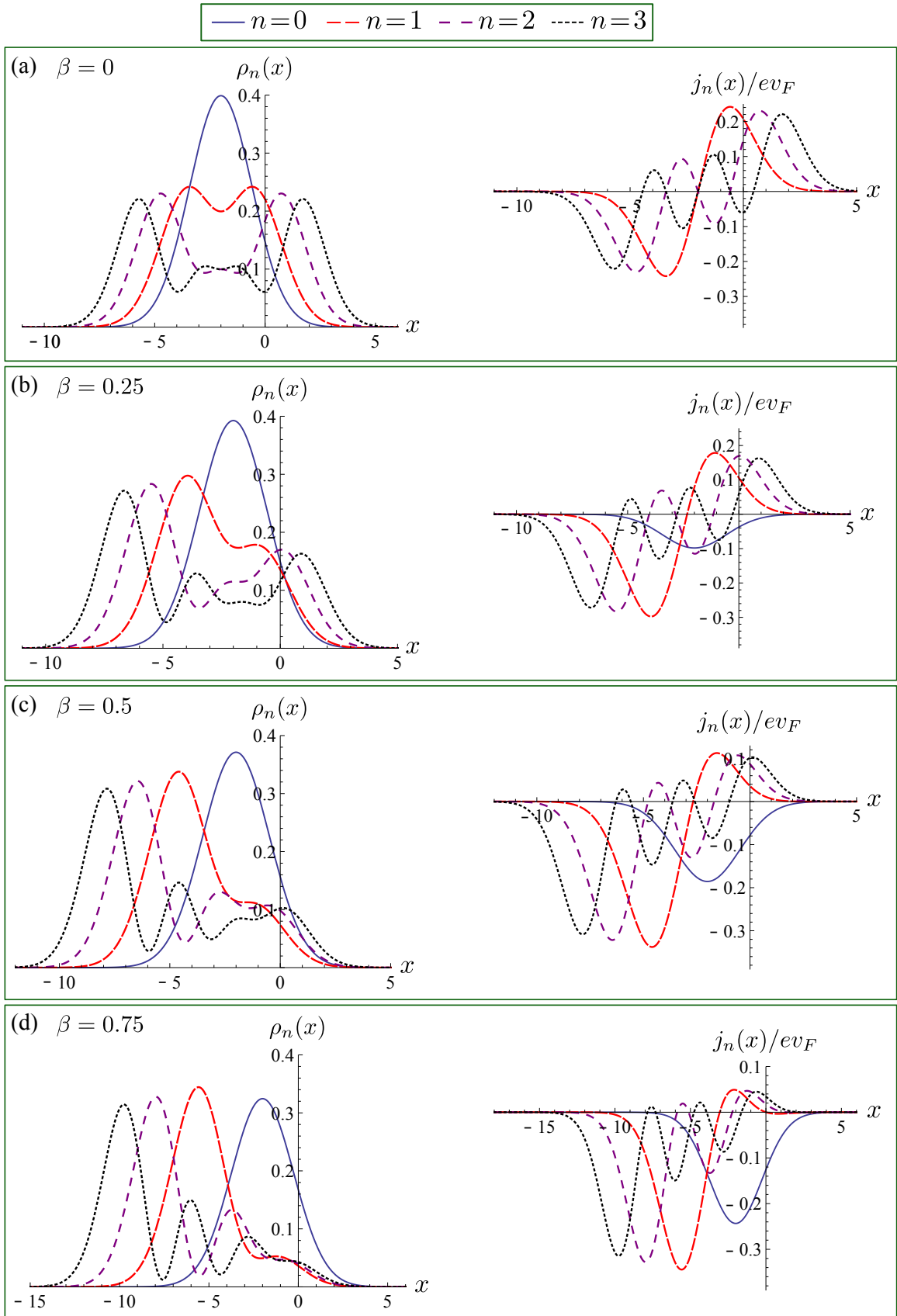


Figure 3: Upper panels show the probability density $\rho_n(x)$ (left-hand) and the y -current density $j_n(x)/ev_F$ (right-hand) for different eigenstates $\bar{\Phi}_n$ and values of β . In all these cases $B = 1/2$, $k = \omega_B = 1$.

as well as the (unitary) shift operators \mathcal{T}^\pm [40], whose explicit action onto the eigenfunctions $\psi_n(\zeta_n)$ is

$$\mathcal{Q}^- \psi_n(\zeta_n) = \mathcal{T}^- \theta_n^- \psi_n(\zeta_n) = \sqrt{n} \psi_{n-1}(\zeta_{n-1}), \quad \mathcal{Q}^+ \psi_n(\zeta_n) = \theta_n^+ \mathcal{T}^+ \psi_n(\zeta_n) = \sqrt{n+1} \psi_{n+1}(\zeta_{n+1}). \quad (17)$$

This means that the operators θ_n^\pm change in a unity the energy level of the eigenstates ψ_n , while the operators \mathcal{T}^\pm shift in a unity the index n of the spacial coordinate ζ_n in the wave function $\psi_n(\zeta_n)$. It is straightforward to verify that $[\mathcal{Q}^-, \mathcal{Q}^+] = 1$.

Now, we define the following operators in terms of θ_n^\pm [34, 36]:

$$\Theta_n^- = \begin{pmatrix} \cos(\delta) \frac{\sqrt{N+2} \theta_n^-}{\sqrt{N+1}} & \eta \sin(\delta) \frac{1}{\sqrt{N+1}} (\theta_n^-)^2 \\ -\eta \sin(\delta) \sqrt{N+1} & \cos(\delta) \theta_n^- \end{pmatrix}, \quad \Theta_n^+ = (\Theta_n^-)^\dagger. \quad (18)$$

Here, $N = \theta_n^+ \theta_n^-$ is the number operator and $\delta \in [0, 2\pi]$ is a parameter that allows to work with either diagonal or non-diagonal matrix operators. This annihilation operator coincides with a given one in [34, 36]. After that, we also define the matrix operators

$$\Theta^- = \mathcal{T}^- \sum_{n=0} \Theta_n^- \mathcal{P}(n), \quad \Theta^+ = (\Theta^-)^\dagger, \quad (19)$$

where $\mathcal{P}(k)$ is a 1-dimensional projection such that [41]

$$\Theta^- \bar{\Phi}_k = \mathcal{T}^- \sum_{n=0} \Theta_n^- (\mathcal{P}(n) \bar{\Phi}_k) = \mathcal{T}^- \sum_{n=0} \delta_{kn} \Theta_n^- \bar{\Phi}_k = \mathcal{T}^- \Theta_k^- \bar{\Phi}_k. \quad (20)$$

We discuss the algebraic relations of these matrix operators in Appendix D.

4.1 Coherent states as eigenstates of Θ^-

The action of the annihilation operator Θ^- on the eigenstates $\bar{\Phi}_n(x, y)$ turns out to be

$$\Theta^- \bar{\Phi}_n(x, y) \equiv \Theta^- \bar{\Phi}_n(\zeta_n, y) = \frac{\exp(i\delta)}{\sqrt{2^{\delta_{1n}}}} \sqrt{n} \bar{\Phi}_{n-1}(\zeta_{n-1}, y), \quad n = 0, 1, 2, \dots \quad (21)$$

By solving the eigenvalue equation

$$\Theta^- \Phi_\alpha(x, y) = \alpha \Phi_\alpha(x, y), \quad \alpha \in \mathbb{C}, \quad (22)$$

where

$$\Phi_\alpha(x, y) = \sum_{n=0}^{\infty} a_n \bar{\Phi}_n(x, y), \quad (23)$$

and using (21), we find the explicit expression for the corresponding coherent states:

$$\Phi_\alpha(x, y) = \frac{1}{\sqrt{2 \exp(|\tilde{\alpha}|^2) - 1}} \left[\bar{\Phi}_0(x, y) + \sum_{n=1}^{\infty} \frac{\sqrt{2} \tilde{\alpha}^n}{\sqrt{n!}} \bar{\Phi}_n(x, y) \right], \quad (24)$$

with $\tilde{\alpha} \equiv \alpha \exp(-i\delta)$, and $\alpha = |\alpha| \exp(i\varphi)$. This means that to work with either a diagonal or non-diagonal annihilation operator Θ^- results in the introduction of a phase factor that affects the eigenvalue α . Actually, the phase of α already corresponds to the classical phase angle [42, 43], *i.e.*, α is a periodic amount that contains information about the cyclic change of the mean value of both the position and the momentum, as will be seen in forthcoming sections.

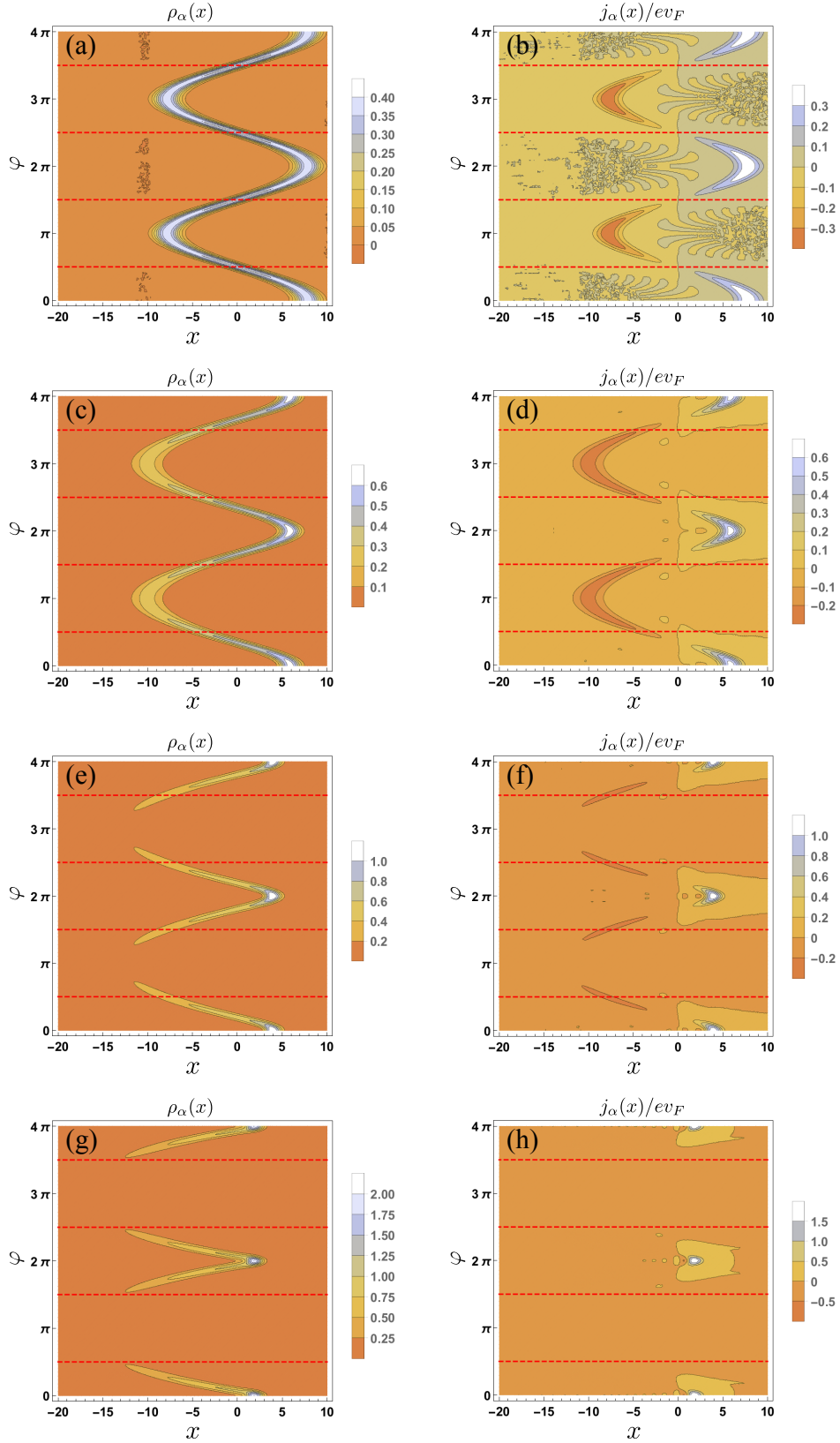


Figure 4: Upper panels show the probability density $\rho_\alpha(x) = |\Psi_\alpha(x, y)|^2$ (left-hand) and the y -current density $j_\alpha(x)/e v_F$ (right-hand) in (25a) for the coherent states $\Psi_\alpha(x, y)$ as functions of the phase φ for different values of β : $\beta = 0$ (a, b), $\beta = 0.25$ (c, d), $\beta = 0.5$ (e, f) and $\beta = 0.75$ (g, h). In all these cases $|\alpha| = 4$, $B = 1/2$, $\omega_B = 1$ and $k = \delta = 0$. Dashed red lines correspond to $\varphi = (2n + 1)\pi/2$, $n = 0, 1, 2, \dots$

4.1.1 Probability and current densities

The corresponding probability and y -current densities for the coherent states $\Psi_\alpha = \mathbb{M}\Phi_\alpha$ read as (see Fig. 4):

$$|\Psi_\alpha(x, y)|^2 = \left[2 \exp(|\tilde{\alpha}|^2) - 1 - 2\beta \Re(\tilde{\alpha}) \sum_{n=0}^{\infty} \frac{|\tilde{\alpha}|^{2n}}{n! \sqrt{n+1}} \right]^{-1} \left[\left| \psi_0^2(\zeta_0) + \left| \sum_{n=1}^{\infty} \frac{\tilde{\alpha}^n}{\sqrt{n!}} \psi_n(\zeta_n) \right|^2 + \left| \sum_{n=1}^{\infty} \frac{\tilde{\alpha}^n}{\sqrt{n!}} \psi_{n-1}(\zeta_n) \right|^2 \right. \right. \\ \left. \left. + 2\Re \left(\sum_{n=1}^{\infty} \frac{\tilde{\alpha}^n}{\sqrt{n!}} \psi_n(\zeta_n) \psi_0(\zeta_0) \right) - 2\beta \Re \left(\sum_{n=1}^{\infty} \frac{\tilde{\alpha}^n}{\sqrt{n!}} \psi_{n-1}(\zeta_n) \psi_0(\zeta_0) + \sum_{m,n=1}^{\infty} \frac{\tilde{\alpha}^{*m} \tilde{\alpha}^n}{\sqrt{m!} n!} \psi_{m-1}(\zeta_n) \psi_n(\zeta_n) \right) \right], \quad (25a)$$

$$\frac{j_\alpha(x)}{e v_F} = \left[2 \exp(|\tilde{\alpha}|^2) - 1 - 2\beta \Re(\tilde{\alpha}) \sum_{n=0}^{\infty} \frac{|\tilde{\alpha}|^{2n}}{n! \sqrt{n+1}} \right]^{-1} \left\{ 2\Re \left(\sum_{n=1}^{\infty} \frac{\tilde{\alpha}^n}{\sqrt{n!}} \psi_{n-1}(\zeta_n) \psi_0(\zeta_0) + \sum_{m,n=1}^{\infty} \frac{\tilde{\alpha}^{*m} \tilde{\alpha}^n}{\sqrt{m!} n!} \psi_{m-1}(\zeta_n) \right) \right. \\ \left. \times \psi_n(\zeta_n) \right) - \beta \left[\psi_0^2(\zeta_0) + \left| \sum_{n=1}^{\infty} \frac{\tilde{\alpha}^n}{\sqrt{n!}} \psi_n(\zeta_n) \right|^2 + \left| \sum_{n=1}^{\infty} \frac{\tilde{\alpha}^n}{\sqrt{n!}} \psi_{n-1}(\zeta_n) \right|^2 + 2\Re \left(\sum_{n=1}^{\infty} \frac{\tilde{\alpha}^n}{\sqrt{n!}} \psi_n(\zeta_n) \psi_0(\zeta_0) \right) \right] \right\}. \quad (25b)$$

For $\beta = 0$ ($\mathcal{E} = 0$), we recover the results discussed in [34]. For $\beta \neq 0$, we can see that the shape of both probability and y -current densities changes as β increases. In a semi-classical interpretation, the eigenvalue α translates as an initial condition with which we can indicate the initial position of an electron along the x -axis for a given time t_0 . On the other hand, when the amount $\beta \rightarrow 1$, the probability density shows a maximum value in a small region in the x -axis, *i.e.*, such behavior suggests that the presence of an electric field would tend to reduce the velocity of the electrons in particular regions along the x axis, so that the probability of finding them there will increase. Meanwhile, the sign of the y -current density indicates the direction in which the electron movement takes place along the y -direction [14]. For $\beta = 0$, such a function has both positive and negative values, so that the electrons move as many times to the positive as the negative direction along the y -axis. As $\beta \rightarrow 1$, small regions in which the current density becomes most positive appear, indicating that when the electron speed reduces, it moves in the positive y -direction.

4.1.2 Heisenberg uncertainty relation

In order to compute the Heisenberg uncertainty relation, we define the following matrix quadrature \mathbb{S}_q and its square as

$$\mathbb{S}_q = \sum_{n=0}^{\infty} (s_q \otimes \mathbb{I}) \mathcal{P}(n), \quad \mathbb{S}_q^2 = \sum_{n=0}^{\infty} (s_q^2 \otimes \mathbb{I}) \mathcal{P}(n), \quad (26)$$

where

$$s_q = \frac{1}{\sqrt{2}i^q} (\mathcal{Q}^- + (-1)^q \mathcal{Q}^+), \quad (27a)$$

$$s_q^2 = \frac{1}{2} [2N + 1 + (-1)^q ((\mathcal{Q}^-)^2 + (\mathcal{Q}^+)^2)], \quad (27b)$$

and $q = 0, 1$. The variance of the operator \mathbb{S}_q is calculated as follows:

$$\sigma_{S_q} = \sqrt{\langle \mathbb{S}_q^2 \rangle - \langle \mathbb{S}_q \rangle^2}. \quad (28)$$

The explicit expressions of $\langle \mathbb{S}_q \rangle$ and $\langle \mathbb{S}_q^2 \rangle$ in the coherent states basis are given in Appendix E. For $q = 0$ ($q = 1$), we have that $\sigma_{S_0} \equiv \sigma_\zeta$ ($\sigma_{S_1} \equiv \sigma_p$), *i.e.*, the variance of the position-like ζ (momentum-like p) operator that fulfills:

$$\sigma_\zeta \sigma_p = \sigma_{S_0} \sigma_{S_1} \geq \frac{1}{2}. \quad (29)$$

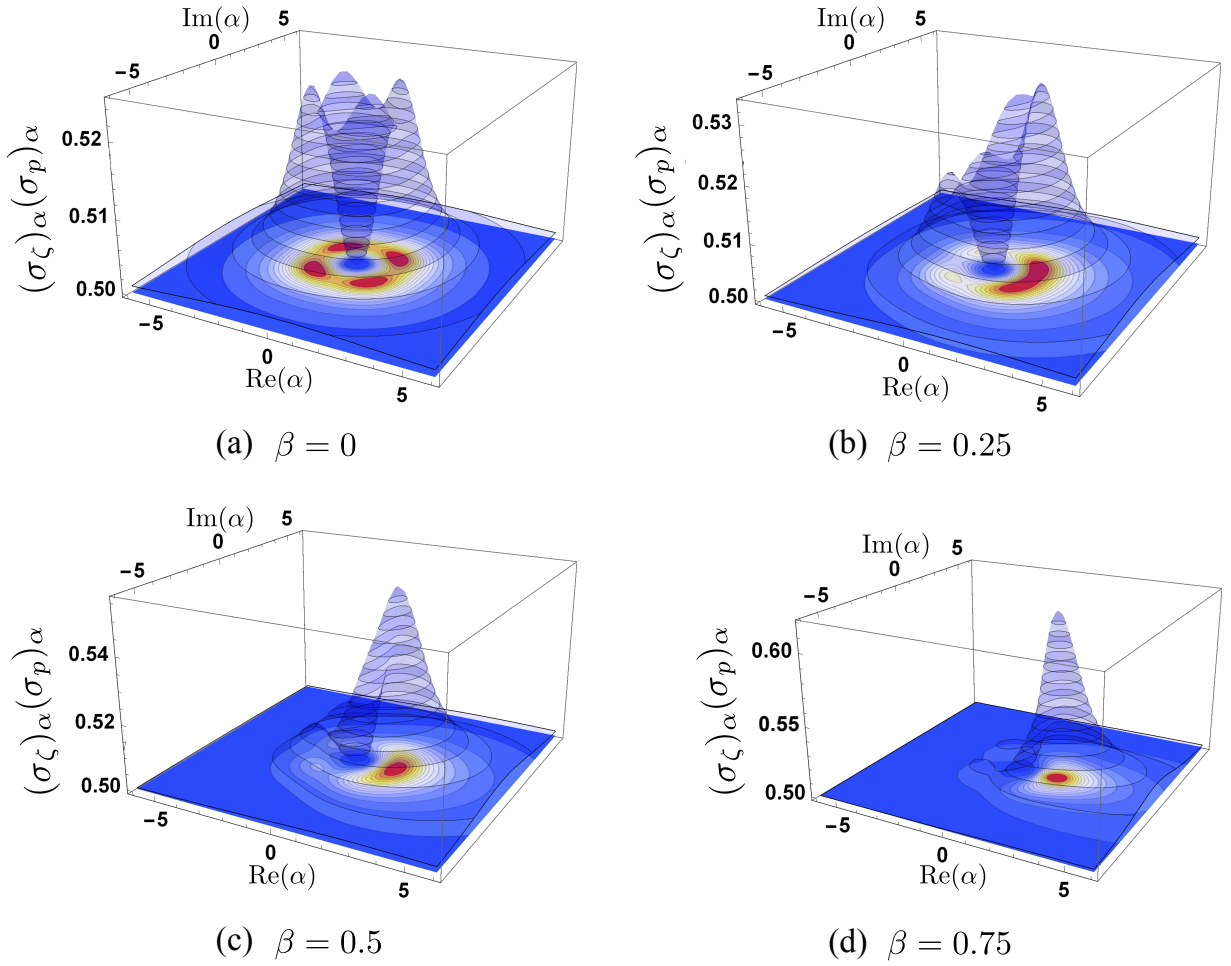


Figure 5: HUR for the coherent states $\Psi_\alpha(x, y)$ as function of the eigenvalue α with $\delta = 0$ for some values of β .

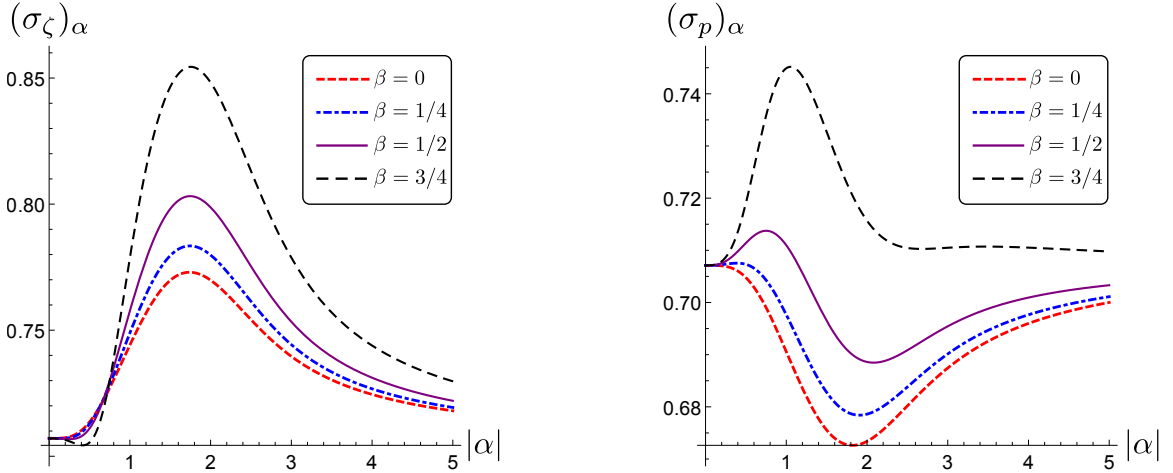


Figure 6: Comparison between the position and momentum variances as function of $|\alpha|$ for different values of β . In general, $\sigma_p \leq \sigma_z$ and as $\beta \rightarrow 1$, σ_z increases.

For the standard coherent states (SCS) of the harmonic oscillator, the equality is verified.

Figure 5 shows that for coherent states $\Psi_\alpha = \mathbb{M}\Phi_\alpha$, the function $\sigma_z \sigma_p$ is greater than $1/2$ for some values of α and φ . In general, the behavior of $\sigma_z \sigma_p$ for small values of $|\alpha|$ depends on the individual variances of the quadratures S_0 (position-like operator) and S_1 (momentum-like operator) on the coherent state basis considered, as shown in figure 5 of Ref. [36]. Additionally,

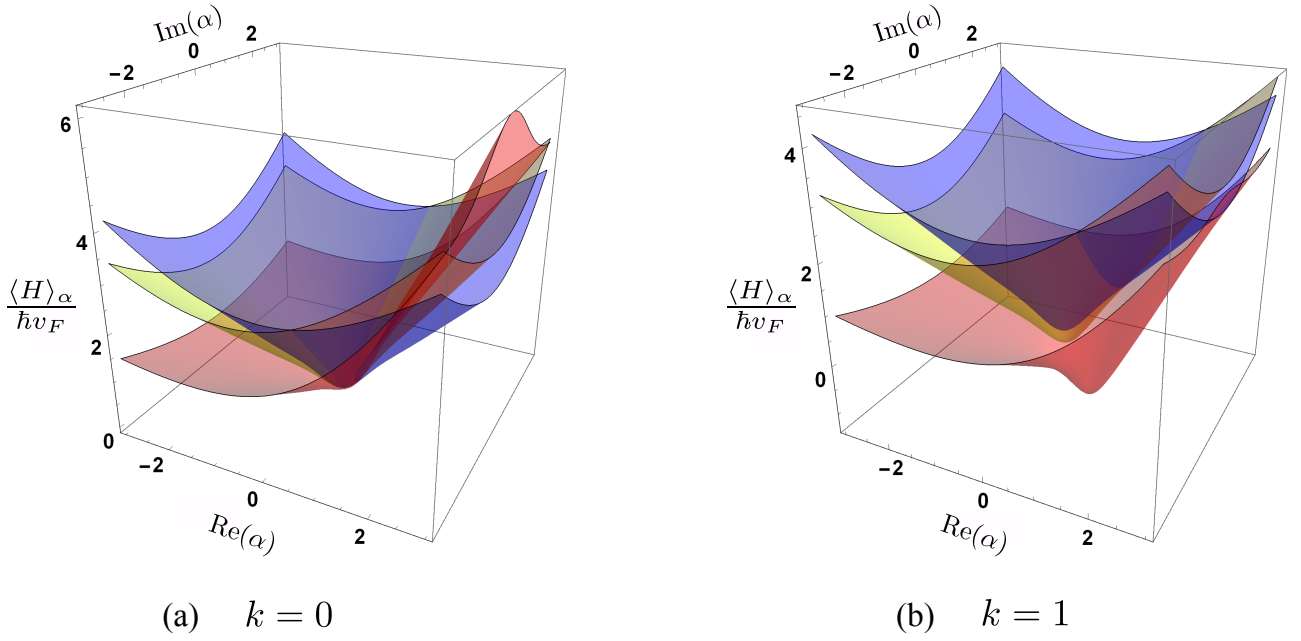


Figure 7: Mean energy $\langle H \rangle_\alpha / \hbar v_F$ as function of α with $\delta = 0$ for the coherent states $\Psi_\alpha(x, y)$ with different values of β : $\beta = 0$ (blue), $\beta = 0.25$ (yellow) and $\beta = 0.75$ (red). In all these cases, we take $B = 1/2$ and $\omega_B = 1$.

for φ close to zero and growing β , the variance σ_p remains less than σ_ζ and when $\beta \sim 1$, $\sigma_\zeta \sigma_p$ reaches its maximum value in the vicinity of $\varphi = 0$ and for small values of $|\alpha|$ (see Fig. 6).

4.1.3 Mean energy value

Recalling that for any linear combination of eigenstates Ψ_n of a Hamiltonian H' with eigenvalues E_n we have that

$$\Psi = \sum_n a_n \Psi_n \implies \langle H' \rangle = \sum_n |a_n|^2 E_n, \quad (30)$$

the mean energy $\langle H \rangle_\alpha$ for the coherent states $\Psi_\alpha(x, y)$ can be expressed as follows:

$$\begin{aligned} \frac{\langle H \rangle_\alpha}{\hbar v_F} = & \left[2 \exp(|\tilde{\alpha}|^2) - 1 - 2\beta \Re(\tilde{\alpha}) \sum_{n=0}^{\infty} \frac{|\tilde{\alpha}|^{2n}}{n! \sqrt{n+1}} \right]^{-1} \left[k\beta (1 - 2 \exp(|\tilde{\alpha}|^2)) \right. \\ & \left. + \frac{2(1 - \beta^2)^{3/4}}{l_B} \sum_{n=1}^{\infty} \frac{|\tilde{\alpha}|^{2n}}{n!} \sqrt{2n} \right]. \end{aligned} \quad (31)$$

As Fig. 7 shows, $\langle H \rangle_\alpha$ is a continuous function of the eigenvalue α , that allows us to assure the semi-classical nature of our results. Furthermore, the mean energy value exhibits a conic shape around the eigenvalue $\alpha = 0$, whose inclination increases as β also does. Actually, this behavior suggests that the presence of an external electric field works as a parameter of tilt for the mean energy. Such behavior is common in 2D DMs that possess tilted (anisotropic) Dirac cones [13, 26, 44].

4.2 Discussion

In comparison with [34], we also obtain an oscillatory-like behavior for the probability and current densities around a middle point x_0 , whose location on x -axis depends on the strength of \mathbf{E} and \mathbf{B} . For the case with the electric field turned off, the function $\rho_\alpha(x)$ has only contributions

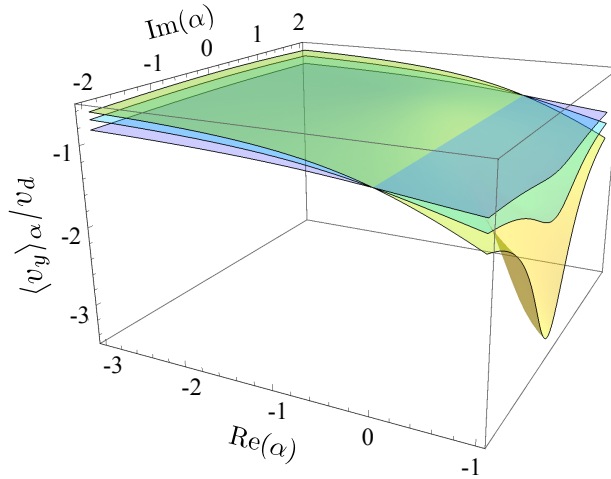


Figure 8: Average velocity in y -direction $\langle v_y \rangle_\alpha / v_d$ as function of α with $\delta = 0$ for the coherent states $\Psi_\alpha(x, y)$ with different values of β : $\beta = 0.25$ (blue), $\beta = 0.5$ (cyan) and $\beta = 0.75$ (yellow). In all these cases, we take $B = 1/2$ and $\omega_B = 1$.

of the spinor components in each sublattice separately, but when the electric field turns on, is affected by a quantity proportional to the current density from the case with \mathcal{E} null. Likewise, while the magnetic field is applied only, the function $j_y(x)$ has contributions of the components mixed and when the electric field appears, the starting current density is affected by an amount proportional to $\rho_\alpha(x)$ from the case with $\mathcal{E} = 0$ (see Eq. (25a) and Fig. 4). Similar results are found for the eigenstates $\Psi_n(x, y)$ (see Eq. (C.2) and Fig. 3).

As was mentioned before, the main role of the coherent states in quantum mechanics is, in general, to describe the behavior of a system in a semi-classical approach, although that aim is not easy for all quantum systems. In our case, when Dirac electrons interact with an external magnetic field only, for a phase variation of the eigenvalue α that characterizes the coherent state, the probability density does not change its shape: a Gaussian distribution on the x -axis. In the added electric field case, the probability density is accumulated in some particular points along the x -direction as φ changes. This means that is more probable to find electrons in certain spatial regions choosing the correct eigenvalue phase. Likewise, the current density changes as the parameter β increases, taking positive values in the points where $|\Psi_\alpha|^2$ is longer on x -axis. Thus, we can assume that in such points electrons not only reduce their group velocity, but also their motion direction changes as a result of the presence of a constant electric field directed along the positive x -axis (Fig. 4). From a semi-classical point of view, an electron in an external magnetic field describes a circular orbit, which is equivalent to being able to detect the particle in wherever place on the trajectory. When an electric field is applied, the charged carriers move in a spiral way giving place to points in which their speed decreases and they can be detected with larger probability (Fig. 1). Furthermore, as the electric field strength increases, such points appear more to the left of the x -axis each time, due to the attractive forces generated by the electric field.

Besides, following [39], the average velocity in y -direction is calculated as

$$\langle v_y \rangle_\alpha = \frac{1}{\hbar} \frac{\partial}{\partial k} \langle H \rangle_\alpha = \left[2 \exp(|\tilde{\alpha}|^2) - 1 - 2\beta \Re(\tilde{\alpha}) \sum_{n=0}^{\infty} \frac{|\tilde{\alpha}|^{2n}}{n! \sqrt{n+1}} \right]^{-1} [v_d (1 - 2 \exp(|\tilde{\alpha}|^2))] . \quad (32)$$

As we can see in Fig. 8, as $|\alpha|$ grows up, the average velocity $|\langle v_y \rangle_\alpha|$ tends to a smaller (bigger) constant value than v_d for $\pi/2 \leq \varphi \leq 3\pi/2$ ($-\pi/4 < \varphi < \pi/4$). The minus sign in $\langle v_y \rangle_\alpha$ indicates the velocity is directed along the negative y -axis.

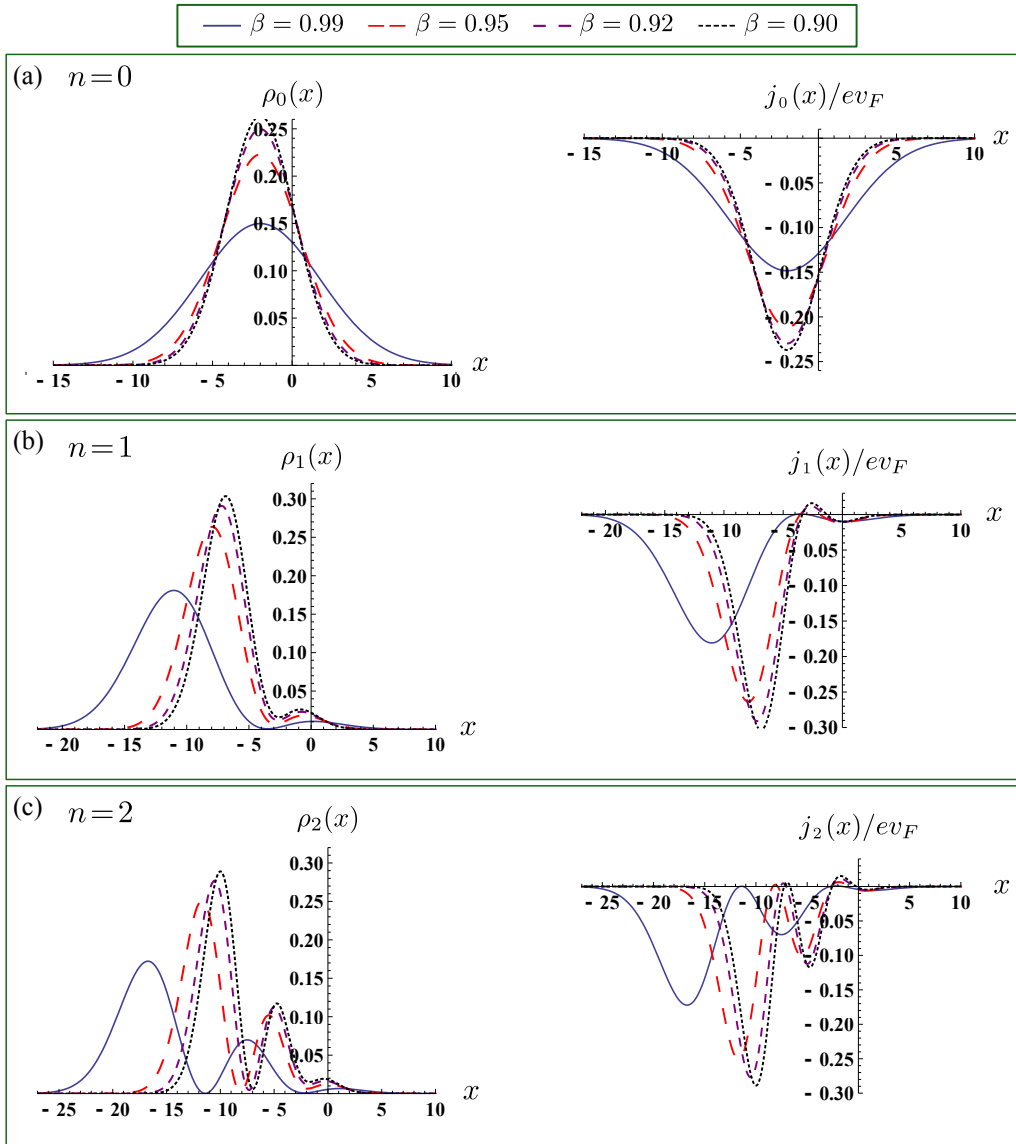


Figure 9: Upper panels show the probability density $\rho_n(x)$ (left-hand) and the y -current density $j_n(x)/ev_F$ (right-hand) for three different Landau levels $n = 0, 1, 2$ and values of β close to 1. In all these cases $B = 1/2$, $k = \omega_B = 1$.

Collapse of Landau levels ($\beta \rightarrow 1$)

Figure 9 shows the behavior of the probability and current densities along the x -axis for the states in Eq. (10) when β takes values close to 1. We can see that while the sign of the function $j_y(x)$ holds negative, the amplitude of the maximum probability for such values is less than when $\beta < 1$ (Fig. 3), indicating that when $\mathcal{E} \approx v_F B/c$, the probability of finding a Dirac particle on the left side of the x -axis decreases.

On the other hand, as the drift velocity v_d approximates to Fermi velocity v_F , the Heisenberg uncertainty relation is longer than $1/2$ only for real values of α (see Figs. 5 and 10), for which the position-like variance σ_ζ remains always larger than the momentum-like one σ_p . Additionally, it is worth to mention that for $\alpha \in \mathbb{C}$ for which the HUR is not equal to $1/2$, the mean energy $\langle H \rangle_\alpha$ is tilted as also β increases (Fig 7), indicating that such values would correspond to a larger mean energy.

In summary, since Landau levels already collapse in the limit value $\mathcal{E}_c = v_F B/c$, our results are not valid close to that critical point due to the bounded states would disappear becoming into scattering states and we would have that $|\langle v_y \rangle_\alpha| > v_d \approx v_F$ [14]. Actually, in [45] the

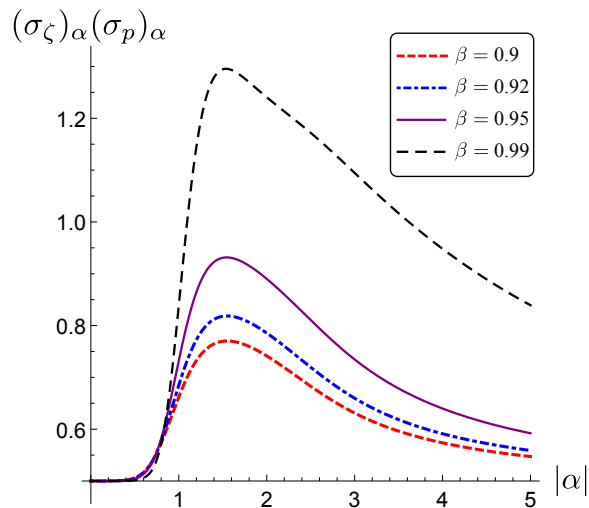


Figure 10: HUR for the coherent states $\Psi_\alpha(x, y)$ as function of $|\alpha|$ for values of β close to 1.

critical value $\beta = 1$ is analyzed showing that existence of no bound states, while for $\beta > 1$, *i.e.* a weak magnetic field, the problem holds solvable and leads to a bit different spectrum behavior [46].

5 Concluding remarks

We have solved the two-dimensional Dirac-Weyl equation with an external electric field by using a clear algebraic method that prevents us to implement techniques of special relativity. Also, we have been able to obtain the known results of the system interacting only with a magnetic field by taking the limit $\beta \rightarrow 0$.

Likewise, we have build the coherent states for a graphene sample on xy -plane interacting with both electric and magnetic fields. In addition, our results are not only in agreement with those of classical mechanics but also allow to establish a model that describes the effects of both fields on charge carriers in a stationary regime through physical quantities such as probability and current densities, Heisenberg uncertainty relation and mean energy. Our main conclusion is that the electric field modifies the location of the quasi-particles in graphene. This semi-classical description could be implemented to analyze electronic or transport properties in graphene or other 2D DMs, as occurs for the so-called Bloch oscillations [39].

Acknowledgments

The authors acknowledge Vít Jakubský and the anonymous referee for their valuable comments to improve this work. M.C.C. acknowledges the CONACyT fellowship 301117. M.O.L. acknowledges to CONACyT for a postdoctoral fellowship.

A Eigenvalues and eigenstates

In order to find the solutions of our problem, we proceed as [47]. Hence, multiplying by $-i\sigma_x$ to the left of Eq. (8), we get:

$$\left[\frac{1}{l_B} \frac{d}{d\xi} \mathbb{I}_2 - i \left(\epsilon_0 - \frac{\beta \xi}{l_B} \right) \sigma_x \mathbb{I}_2 + i \frac{\xi}{l_B} \sigma_x \sigma_y \right] \Psi(\xi) = 0, \quad (\text{A.1})$$

where $\epsilon_0 = E/\hbar v_F + k\beta$. Differentiating this equation with respect to ξ and manipulating a bit, we obtain the following equation

$$\left[\left(\frac{d^2}{d\xi^2} + (\epsilon_0 l_B - \beta\xi)^2 - \xi^2 \right) \mathbb{I}_2 + i(\sigma_x \beta + \sigma_x \sigma_y) \right] \Psi(\xi) = 0, \quad (\text{A.2})$$

whose solutions can be expressed as $\Psi(\xi)_\lambda = \psi_\lambda(\xi)\chi_\lambda$, where χ_λ is an eigenvector of the complex symmetric matrix $\mathbb{K} = i(\sigma_x \beta + \sigma_x \sigma_y)$ with eigenvalue λ and $\psi_\lambda(\xi)$ is a scalar function that satisfies the differential equation

$$\left[\frac{d^2}{d\xi^2} + (\epsilon_0 l_B - \beta\xi)^2 - \xi^2 + \lambda \right] \psi_\lambda(\xi) = 0, \quad (\text{A.3})$$

In order to simplify the above equation, the variable ζ is defined as

$$\zeta = \xi(1 - \beta^2)^{1/4} + \frac{\beta\epsilon_0 l_B}{(1 - \beta^2)^{3/4}} = \frac{(1 - \beta^2)^{1/4}}{l_B} \left[x + l_B^2 k + \frac{\beta\epsilon_0 l_B^2}{1 - \beta^2} \right], \quad (\text{A.4})$$

where β must fulfill the condition $0 \leq \beta < 1$ for keeping real values of ζ and prevent indeterminacy. Likewise, this implies that $v_d = \mathcal{E}c/B < v_F$, in contrast with the classical drift velocity, in which there is no restriction for the electric field strength. Hence, we obtain the Weber equation

$$\left[\frac{d^2}{d\zeta^2} - \zeta^2 + \frac{\epsilon_0^2 l_B^2}{(1 - \beta^2)^{3/2}} + \frac{\lambda}{(1 - \beta^2)^{1/2}} \right] \psi_\lambda(\zeta) = 0, \quad (\text{A.5})$$

where the dimensionless potential $V_\beta(\zeta)$ can be identified as

$$V_\beta(\zeta) = \zeta^2 - \frac{\lambda}{(1 - \beta^2)^{1/2}}. \quad (\text{A.6})$$

On the other hand, the eigenvalues λ of the matrix \mathbb{K} turn out to be $\sigma(\mathbb{K}) = \{\lambda_k = (-1)^k(1 - \beta^2)^{1/2}\}$ with $k = 1, 2$, while the corresponding normalized eigenvectors are given by

$$S = \left\{ \chi_{\lambda_1} = \frac{1}{\sqrt{2}} \begin{pmatrix} \sqrt{C_+} \\ -i\sqrt{C_-} \end{pmatrix}, \quad \chi_{\lambda_2} = \frac{1}{\sqrt{2}} \begin{pmatrix} -\sqrt{C_-} \\ i\sqrt{C_+} \end{pmatrix} \right\}, \quad (\text{A.7})$$

where $C_\pm = 1 \pm (1 - \beta^2)^{1/2}$. Substituting the eigenvalues λ_k in Eq. (A.5) and taking $\psi_\lambda(\zeta) = \exp(-\zeta^2/2) f_\lambda(\zeta)$, one gets the following ODE:

$$f_\lambda''(\zeta) - 2\zeta f_\lambda'(\zeta) + \left(\frac{\epsilon_0^2 l_B^2}{(1 - \beta^2)^{3/2}} - 1 + (-1)^k \right) f_\lambda(\zeta) = 0, \quad k = 1, 2. \quad (\text{A.8})$$

From here, the results shown in Eqs. (9)-(12) are followed. Besides, the procedure implemented to solve (8) has also been successfully applied for reproducing some results in [48].

B Matrix \mathbb{M}

In this part, we focus on describing some features of matrix \mathbb{M} in Eq. (11).

Since \mathbb{M} is a hermitian matrix, it can be diagonalized, *i.e.*, there is a diagonal matrix \mathbb{D} and a unitary matrix \mathbb{U} such that $\mathbb{M} = \mathbb{U}\mathbb{D}\mathbb{U}^{-1}$.

After finding the \mathbb{M} -eigenvalues,

$$\sigma(\mathbb{M}) = \left\{ \mu_k = \frac{\sqrt{C_+} + (-1)^k \sqrt{C_-}}{\sqrt{2}} \right\}, \quad k = 1, 2, \quad (\text{B.1})$$

and the corresponding eigenvectors,

$$S = \left\{ \chi_{\mu_1} = \frac{1}{\sqrt{2}} \begin{pmatrix} 1 \\ i \end{pmatrix}, \quad \chi_{\mu_2} = \frac{1}{\sqrt{2}} \begin{pmatrix} i \\ 1 \end{pmatrix} \right\}, \quad (\text{B.2})$$

it follows that matrix \mathbb{M} can be expressed as

$$\mathbb{M} = \mathbb{U}(\pi/4)\mathbb{D}\mathbb{U}^{-1}(\pi/4), \quad (\text{B.3})$$

where $\mathbb{D} = \text{diag}(\mu_1, \mu_2)$ and $\mathbb{U}(\tau) = \exp(i\tau\sigma_x)$. Therefore, \mathbb{M} is obtained from rotations about the x -axis.

C Probability and current densities

We can obtain the expressions for the probability density $\rho_n(x) = |\Psi_n(x)|^2$ and the current density $j_{x/y}(x) = ev_{\text{F}}\Psi_n^\dagger(x)\sigma_{x/y}\Psi_n(x)$ in the x/y -direction by identifying the following relations:

$$\mathbb{M}^\dagger\mathbb{M} = \mathbb{I}_2 - \beta\sigma_y, \quad (\text{C.1a})$$

$$\mathbb{M}^\dagger\sigma_x\mathbb{M} = \sqrt{1 - \beta^2}\sigma_x, \quad (\text{C.1b})$$

$$\mathbb{M}^\dagger\sigma_y\mathbb{M} = \sigma_y - \beta\mathbb{I}_2. \quad (\text{C.1c})$$

Thus, the probability density $\rho_n(x)$ and the current densities $j_{x/y}(x)$ turn out to be, respectively:

$$\rho_n(x) = |\bar{\Phi}_n(x, y)|^2 - \beta\bar{\Phi}_n^\dagger(x, y)\sigma_y\bar{\Phi}_n(x, y), \quad (\text{C.2a})$$

$$j_x(x) = 0, \quad (\text{C.2b})$$

$$j_y(x) = ev_{\text{F}}\bar{\Phi}_n^\dagger(x, y)\sigma_y\bar{\Phi}_n(x, y) - ev_{\text{d}}|\bar{\Phi}_n(x, y)|^2. \quad (\text{C.2c})$$

Besides, if s represents a scalar operator associated to any observable quantity that has been promoted to a matrix one through the relation $s \rightarrow \mathbb{S} = s \otimes \mathbb{I}$, we have that

$$\langle \mathbb{S} \rangle = \langle \Psi_n | \mathbb{S} | \Psi_n \rangle = \langle \Phi_n | \mathbb{S} | \Phi_n \rangle - \beta \langle \Phi_n | s \sigma_y | \Phi_n \rangle. \quad (\text{C.3})$$

D Matrix operators Θ^\pm

The action of the matrix operators defined in Eq. (18) on the eigenstates $\bar{\Phi}_n(x, y)$ is given by:

$$\Theta^- \bar{\Phi}_n(x, y) \equiv \Theta^- \bar{\Phi}_n(\zeta_n, y) = \frac{\exp(i\delta)}{\sqrt{2^{\delta_{1n}}}} \sqrt{n} \bar{\Phi}_{n-1}(\zeta_{n-1}, y), \quad n = 0, 1, 2, \dots, \quad (\text{D.1a})$$

$$\Theta^+ \bar{\Phi}_n(x, y) \equiv \Theta^- \bar{\Phi}_n(\zeta_n, y) = \exp(-i\delta) \sqrt{n+1} \bar{\Phi}_{n+1}(\zeta_{n+1}, y), \quad n = 1, 2, 3, \dots \quad (\text{D.1b})$$

According to these relations, the operator Θ^+ cannot be considered as a creation operator since its action on the state $\bar{\Phi}_0$ does not generate other eigenstate of the Hilbert space \mathcal{H} . As a consequence, the commutation relation $[\Theta^-, \Theta^+] = \mathbb{I}_2$ only fulfills for $n \geq 2$.

On the other hand, if we consider the operator

$$\tilde{\Theta}^+ = \exp(-i\delta) \sum_{n=0} \begin{pmatrix} \theta_n^+ \frac{\sqrt{N+2}}{\sqrt{N+1}} & -i\eta\sqrt{N+1} \\ i\eta(\theta_n^+)^2 \frac{1}{\sqrt{N+1}} & \theta_n^+ \end{pmatrix} \mathcal{P}(n)\mathcal{T}^+, \quad (\text{D.2})$$

such that

$$\tilde{\Theta}^+ \bar{\Phi}_n(x, y) \equiv \tilde{\Theta}^+ \bar{\Phi}_n(\zeta_n, y) = \sqrt{2^{(2-\delta_{0n})}} \exp(-i\delta) \sqrt{n+1} \bar{\Phi}_{n+1}(\zeta_{n+1}, y), \quad n = 0, 1, 2, \dots, \quad (\text{D.3})$$

we would be able to obtain excited states from the fundamental $\bar{\Phi}_0$ as follows:

$$\bar{\Phi}_k(x, y) \equiv \bar{\Phi}_k(\zeta_k, y) = \frac{\exp(ik\delta)}{\sqrt{2^{(2k-1)}k!}} (\tilde{\Theta}^+)^k \bar{\Phi}_0(\zeta_0, y), \quad k = 1, 2, 3, \dots \quad (\text{D.4})$$

This fact shows that, although $\tilde{\Theta}^+$ is not the adjoint of Θ^- , it works as a creation operator. Furthermore, it is straightforward to verify that

$$[\Theta^-, \tilde{\Theta}^+] \bar{\Phi}_n = c(n) \bar{\Phi}_n, \quad c(n) = \begin{cases} 1, & n = 0, \\ 3, & n = 1, \\ 2, & \text{otherwise.} \end{cases} \quad (\text{D.5})$$

Hence, these results suggest that, up to a constant factor, $\tilde{\Theta}^+$ and Θ^- would be linked to the so-called \mathcal{D} pseudo-bosonic operators [49–53] that arise by modifying the canonical commutation relation $[c, c^\dagger] = 1$, which is replaced with a similar commutation rule, namely, $[a, b] = 1$ where $b \neq a^\dagger$. This discussion takes relevance when, for instance, the construction of coherent states is performed by the Perelomov group theoretical approach [54], in which the algebraic structure of the ladder operators is required.

E Heisenberg uncertainty relation

Using the states in Eq. (24) and according to (C.3), the mean values of the operators \mathbb{S}_q and \mathbb{S}_q^2 are, respectively (see Fig. 5):

$$\langle \mathbb{S}_q \rangle_\alpha = \frac{1}{\sqrt{2}i^q} \left[2 \exp(|\tilde{\alpha}|^2) - 1 - 2\beta \Re(\tilde{\alpha}) \sum_{n=0}^{\infty} \frac{|\tilde{\alpha}|^{2n}}{n! \sqrt{n+1}} \right]^{-1} \left[(\tilde{\alpha} + (-1)^q \tilde{\alpha}^*) \left(\exp(|\tilde{\alpha}|^2) + \sum_{n=1}^{\infty} \frac{|\tilde{\alpha}|^{2n}}{\sqrt{(n-1)!(n+1)!}} \right) - \beta \left((\tilde{\alpha}^2 + (-1)^q \tilde{\alpha}^{*2}) \sum_{n=0}^{\infty} \frac{|\tilde{\alpha}|^{2n}}{n! \sqrt{n+2}} + (1 + (-1)^q) \sum_{n=1}^{\infty} \frac{|\tilde{\alpha}|^{2n}}{n!} \sqrt{n} \right) \right], \quad (\text{E.1a})$$

$$\langle \mathbb{S}_q^2 \rangle_\alpha = \frac{1}{2} \left[2 \exp(|\tilde{\alpha}|^2) - 1 - 2\beta \Re(\tilde{\alpha}) \sum_{n=0}^{\infty} \frac{|\tilde{\alpha}|^{2n}}{n! \sqrt{n+1}} \right]^{-1} \left\{ 1 + 4|\tilde{\alpha}|^2 \exp(|\tilde{\alpha}|^2) + (-1)^q (\tilde{\alpha}^2 + \tilde{\alpha}^{*2}) \right. \\ \times \left(\exp(|\tilde{\alpha}|^2) + \sum_{n=1}^{\infty} \frac{\sqrt{n+1} |\tilde{\alpha}|^{2n}}{\sqrt{(n-1)!(n+2)!}} \right) - \beta \left[(\tilde{\alpha} + \tilde{\alpha}^*) \left(\sum_{n=0}^{\infty} \frac{|\tilde{\alpha}|^{2n}}{n! \sqrt{n+1}} (2n+1) \right) \right. \\ \left. \left. + (-1)^q \sum_{n=1}^{\infty} \frac{|\tilde{\alpha}|^{2n}}{\sqrt{n!(n-1)!}} \right) + (-1)^q (\tilde{\alpha}^3 + \tilde{\alpha}^{*3}) \sum_{n=0}^{\infty} \frac{|\tilde{\alpha}|^{2n}}{n! \sqrt{n+3}} \right] \left. \right\}. \quad (\text{E.1b})$$

F Completeness relation

Let us consider the Hilbert space \mathcal{H} spanned by the DW eigenstates, $\mathcal{H} = \text{span}\{\bar{\Phi}_n | n = 0, 1, 2, \dots\}$, which fulfill the completeness relation

$$|\bar{\Phi}_0\rangle \langle \bar{\Phi}_0| + \sum_{n=1}^{\infty} |\bar{\Phi}_n\rangle \langle \bar{\Phi}_n| \equiv \mathbb{I}_2. \quad (\text{F.1})$$

By defining $r = |\alpha|^2$, we take the measure as:

$$d\mu(\alpha) = \frac{2 \exp(r^2) - 1}{2\pi} r \exp(r^2) dr d\theta, \quad (\text{F.2})$$

we obtain the overcompleteness relation of the coherent states as follows:

$$\begin{aligned} & \frac{|\bar{\Phi}_0\rangle \langle \bar{\Phi}_0|}{2} + \int_{\mathbb{C}} d\mu(\alpha) |\bar{\Phi}_n\rangle \langle \bar{\Phi}_n| \\ &= \frac{|\bar{\Phi}_0\rangle \langle \bar{\Phi}_0|}{2} + \int_{\mathbb{C}} \frac{d\mu(\alpha)}{2 \exp(r^2) - 1} \left[|\bar{\Phi}_0\rangle + \sum_{n=1}^{\infty} \frac{\sqrt{2}\tilde{\alpha}^n}{n!} |\bar{\Phi}_n\rangle \right] \left[\langle \bar{\Phi}_0| + \sum_{m=1}^{\infty} \frac{\sqrt{2}\tilde{\alpha}^m}{m!} \langle \bar{\Phi}_m| \right] \\ &= \frac{|\bar{\Phi}_0\rangle \langle \bar{\Phi}_0|}{2} + \frac{1}{2\pi} \int_0^{\infty} \int_0^{2\pi} \left[|\bar{\Phi}_0\rangle \langle \bar{\Phi}_0| + \sum_{n=1}^{\infty} \frac{\sqrt{2}}{\sqrt{n!}} |\bar{\Phi}_n\rangle \langle \bar{\Phi}_0| r^n e^{in\theta} \right. \\ & \quad \left. + \sum_{m=1}^{\infty} \frac{\sqrt{2}}{\sqrt{m!}} |\bar{\Phi}_0\rangle \langle \bar{\Phi}_m| r^m e^{-im\theta} + \sum_{n,m=1}^{\infty} \frac{2}{\sqrt{n!m!}} |\bar{\Phi}_n\rangle \langle \bar{\Phi}_m| r^{n+m} e^{i(n-m)\theta} \right] r \exp(r^2) dr d\theta. \end{aligned} \quad (\text{F.3})$$

Taking the variable change $t = r^2$ and integrating over θ and t , we get finally:

$$\frac{|\bar{\Phi}_0\rangle \langle \bar{\Phi}_0|}{2} + \int_{\mathbb{C}} d\mu(\alpha) |\bar{\Phi}_n\rangle \langle \bar{\Phi}_n| = |\bar{\Phi}_0\rangle \langle \bar{\Phi}_0| + \sum_{n=1}^{\infty} \frac{|\bar{\Phi}_n\rangle \langle \bar{\Phi}_n|}{n!} \Gamma(n+1), \quad (\text{F.4})$$

which reduces to Eq. (F.1).

References

- [1] K. S. Novoselov, A. K. Geim, S. V. Morozov, D. Jiang, Y. Zhang, S. V. Dubonos, I. V. Grigorieva, and A. A. Firsov, “Electric field effect in atomically thin carbon films,” *Science*, vol. 306, no. 5696, pp. 666–669, 2004.
- [2] K. S. Novoselov, A. K. Geim, S. V. Morozov, D. Jiang, M. Katsnelson, I. Grigorieva, S. V. Dubonos, and A. A. Firsov, “Two-dimensional gas of massless Dirac fermions in graphene,” *Nature*, vol. 438, no. 7065, p. 197, 2005.
- [3] A. K. Geim and K. S. Novoselov, “The rise of graphene,” *Nature Materials*, vol. 6, no. 3, pp. 183–191, 2007.
- [4] M. I. Katsnelson, “Graphene: carbon in two dimensions,” *Materials Today*, vol. 10, no. 1, pp. 20 – 27, 2007.
- [5] A. H. Castro Neto, F. Guinea, N. M. R. Peres, K. S. Novoselov, and A. K. Geim, “The electronic properties of graphene,” *Rev. Mod. Phys.*, vol. 81, pp. 109–162, Jan 2009.
- [6] M. O. Goerbig, “Electronic properties of graphene in a strong magnetic field,” *Rev. Mod. Phys.*, vol. 83, pp. 1193–1243, 2011.
- [7] G. G. Naumis, S. Barraza-Lopez, M. Oliva-Leyva, and H. Terrones, “Electronic and optical properties of strained graphene and other strained 2D materials: a review,” *Reports on Progress in Physics*, vol. 80, p. 096501, aug 2017.
- [8] S. Katayama, A. Kobayashi, and Y. Suzumura, “Electronic properties close to Dirac cone in two-dimensional organic conductor α -(BEDT-TTF) $_2$ I $_3$,” *The European Physical Journal B*, vol. 67, pp. 139–148, Jan 2009.

- [9] M. Z. Hasan and C. L. Kane, “Colloquium: Topological insulators,” *Rev. Mod. Phys.*, vol. 82, pp. 3045–3067, Nov 2010.
- [10] X.-L. Qi and S.-C. Zhang, “Topological insulators and superconductors,” *Rev. Mod. Phys.*, vol. 83, pp. 1057–1110, Oct 2011.
- [11] K. Kajita, Y. Nishio, N. Tajima, Y. Suzumura, and A. Kobayashi, “Molecular Dirac Fermion Systems –Theoretical and Experimental Approaches,” *Journal of the Physical Society of Japan*, vol. 83, no. 7, p. 072002, 2014.
- [12] V. Jakubský and M. Tušek, “Dispersionless wave packets in Dirac materials,” *Annals of Physics*, vol. 378, pp. 171 – 182, 2017.
- [13] M. Oliva-Leyva and C. Wang, “Magneto-optical conductivity of anisotropic two-dimensional Dirac-Weyl materials,” *Annals of Physics*, vol. 384, pp. 61 – 70, 2017.
- [14] Ş. Kuru, J. Negro, and L. M. Nieto, “Exact analytic solutions for a Dirac electron moving in graphene under magnetic fields,” *Journal of Physics: Condensed Matter*, vol. 21, no. 45, p. 455305, 2009.
- [15] B. Midya and D. J. Fernández, “Dirac electron in graphene under supersymmetry generated magnetic fields,” *Journal of Physics A: Mathematical and Theoretical*, vol. 47, no. 28, p. 285302, 2014.
- [16] V. Jakubský and D. Krejčířík, “Qualitative analysis of trapped Dirac fermions in graphene,” *Annals of Physics*, vol. 349, pp. 268–287, 2014.
- [17] V. Jakubský, “Spectrally isomorphic Dirac systems: Graphene in an electromagnetic field,” *Physical Review D*, vol. 91, no. 4, p. 045039, 2015.
- [18] M. Castillo-Celeita and D. J. Fernández C, “Dirac electron in graphene with magnetic fields arising from first-order intertwining operators,” *Journal of Physics A: Mathematical and Theoretical*, vol. 53, no. 3, p. 035302, 2020.
- [19] M. Eshghi and H. Mehraban, “Exact solution of the Dirac-Weyl equation in graphene under electric and magnetic fields,” *Comptes Rendus Physique*, vol. 18, no. 1, pp. 47–56, 2017.
- [20] R. R. Hartmann, N. J. Robinson, and M. E. Portnoi, “Smooth electron waveguides in graphene,” *Physical Review B*, vol. 81, no. 24, p. 245431, 2010.
- [21] J. M. Pereira Jr, V. Mlinar, F. M. Peeters, and P. Vasilopoulos, “Confined states and direction-dependent transmission in graphene quantum wells,” *Physical Review B*, vol. 74, no. 4, p. 045424, 2006.
- [22] N. M. R. Peres and E. V. Castro, “Algebraic solution of a graphene layer in transverse electric and perpendicular magnetic fields,” *Journal of Physics: Condensed Matter*, vol. 19, no. 40, p. 406231, 2007.
- [23] C.-L. Ho and P. Roy, “Dirac equation with complex potentials,” *Modern Physics Letters A*, vol. 29, no. 40, p. 1450210, 2014.
- [24] V. Lukose, R. Shankar, and G. Baskaran, “Novel electric field effects on Landau levels in graphene,” *Physical review letters*, vol. 98, no. 11, p. 116802, 2007.

- [25] L. Z. Tan, C.-H. Park, and S. G. Louie, “Graphene Dirac fermions in one-dimensional inhomogeneous field profiles: Transforming magnetic to electric field,” *Physical Review B*, vol. 81, no. 19, p. 195426, 2010.
- [26] J. Sári, M. O. Goerbig, and C. Tóke, “Magneto-optics of quasirelativistic electrons in graphene with an inplane electric field and in tilted dirac cones in α -(BEDT-TTF) $_2$ I $_3$,” *Physical Review B*, vol. 92, no. 3, p. 035306, 2015.
- [27] N. Gu, M. Rudner, A. Young, P. Kim, and L. Levitov, “Collapse of Landau Levels in Gated Graphene Structures,” *Phys. Rev. Lett.*, vol. 106, p. 066601, Feb 2011.
- [28] P. Ghosh and P. Roy, “Collapse of Landau levels in graphene under uniaxial strain,” *Materials Research Express*, vol. 6, no. 12, p. 125603, 2019.
- [29] E. Schrödinger, “Der stetige Übergang von der Mikro-zur Makromechanik,” *Naturwissenschaften*, vol. 14, no. 28, pp. 664–666, 1926.
- [30] J. R. Klauder and B.-S. Skagerstam, *Coherent states: applications in physics and mathematical physics*. World Scientific Pub Co Inc, 1985.
- [31] S. T. Ali, J.-P. Antoine, and J.-P. Gazeau, *Coherent states, wavelets and their generalizations*. Theoretical and Mathematical Physics, Springer-Verlag New York, 2 ed., 2014.
- [32] K. Zelaya, S. Dey, and V. Hussin, “Generalized squeezed states,” *Physics Letters A*, vol. 382, no. 47, pp. 3369–3375, 2018.
- [33] M. Castillo-Celeita, E. Díaz-Bautista, and D. J. Fernández, “Polynomial Heisenberg algebras, multiphoton coherent states and geometric phases,” *Physica Scripta*, vol. 94, no. 4, p. 045203, 2019.
- [34] E. Díaz-Bautista and D. J. Fernández, “Graphene coherent states,” *The European Physical Journal Plus*, vol. 132, no. 11, p. 499, 2017.
- [35] E. Díaz-Bautista, J. Negro, and L. M. Nieto, “Partial coherent states in graphene,” *Journal of Physics: Conference Series*, vol. 1194, p. 012025, Apr 2019.
- [36] E. Díaz-Bautista, Y. Concha-Sánchez, and A. Raya, “Barut–Girardello coherent states for anisotropic 2D-Dirac materials,” *Journal of Physics: Condensed Matter*, vol. 31, p. 435702, jul 2019.
- [37] J. D. Jackson, *Classical electrodynamics*. New York, NY: Wiley, 3rd ed. ed., 1999.
- [38] J. M. Ziman, *Principles of the Theory of Solids*. Cambridge University Press, 2 ed., 1972.
- [39] T. Huang, R. Chen, T. Ma, L.-G. Wang, and H.-Q. Lin, “Electronic Bloch oscillation in a pristine monolayer graphene,” *Physics Letters A*, vol. 382, no. 42, pp. 3086 – 3089, 2018.
- [40] Tomasz Goliński, “Factorization method on time scales,” *Applied Mathematics and Computation*, vol. 347, pp. 354 – 359, 2019.
- [41] H. Isozaki and E. Korotyaev, “Inverse Problems, Trace Formulae for Discrete Schrödinger Operators,” *Annales Henri Poincaré*, vol. 13, no. 4, pp. 751–788, 2012.
- [42] P. Carruthers and M. M. Nieto, “Coherent states and the number-phase uncertainty relation,” *Physical Review Letters*, vol. 14, no. 11, p. 387, 1965.

- [43] M. W. Noel and C. R. Stroud Jr, “Excitation of an atomic electron to a coherent superposition of macroscopically distinct states,” *Physical Review Letters*, vol. 77, no. 10, p. 1913, 1996.
- [44] J. Sári, C. Tóke, and M. O. Goerbig, “Magnetoplasmons of the tilted anisotropic Dirac cone material α -(BEDT-TTF) $_2$ I $_3$,” *Physical Review B*, vol. 90, no. 15, p. 155446, 2014.
- [45] J.-Y. Cheng, “Exact Solutions Describing Collapse of Landau Levels in Graphene,” *Few-Body Systems*, vol. 54, pp. 1931–1935, Nov 2013.
- [46] D. Nath and P. Roy, “Dirac oscillator in perpendicular magnetic and transverse electric fields,” *Annals of Physics*, vol. 351, pp. 13 – 21, 2014.
- [47] J. Oertel, “Solutions of the Dirac equation in spacetime-dependent electric fields,” Master’s thesis, University of Duisburg-Essen, Freiberg, Germany, 2014.
- [48] T. Morinari, T. Himura, and T. Tohyama, “Possible Verification of Tilted Anisotropic Dirac Cone in α -(BEDT-TTF) $_2$ I $_3$ Using Interlayer Magnetoresistance,” *Journal of the Physical Society of Japan*, vol. 78, no. 2, p. 023704, 2009.
- [49] D. A. Trifonov, “Pseudo-Boson Coherent and Fock States,” *preprint arXiv:0902.3744*, 2009.
- [50] F. Bagarello, “More mathematics for pseudo-bosons,” *Journal of Mathematical Physics*, vol. 54, no. 6, p. 063512, 2013.
- [51] F. Bagarello, “From self-adjoint to non-self-adjoint harmonic oscillators: Physical consequences and mathematical pitfalls,” *Phys. Rev. A*, vol. 88, p. 032120, 2013.
- [52] F. Bagarello, J.-P. Gazeau, F. H. Szafraniec, and M. Znojil, *Non-selfadjoint operators in quantum physics: Mathematical aspects*. John Wiley & Sons, 2015.
- [53] F. Bagarello, “A concise review of pseudobosons, pseudofermions, and their relatives,” *Theoretical and Mathematical Physics*, vol. 193, no. 2, pp. 1680–1693, 2017.
- [54] A. M. Perelomov, “Coherent states for arbitrary Lie group,” *Communications in Mathematical Physics*, vol. 26, no. 3, pp. 222–236, 1972.